electronics

MDPI

Article

Design and Analysis of the Model Based Control System for an MRE Axisymmetric Actuator

Paweł Czopek * and Jakub Bernat

Institute of Automatic Control and Robotics, Poznan University of Technology, Piotrowo 3A, 60-965 Poznan, Poland; jakub.bernat@put.poznan.pl
* Correspondence: pawel.czopek@put.poznan.pl

Abstract: The magnetorheological elastomer membrane is an interesting kind of smart material that is gaining new innovative applications. This work is focused on the design of the control system for magnetorheological elastomer actuators. In general, the plant is characterized by fast oscillations and slow drift. Therefore, controllers utilize the described features to obtain the solution aimed at, which makes them unique. We analyze two approaches based on output feedback with state estimation. The control algorithms have different observers to estimate the state. The first is a Linear Extended State Observer, which is applied to reject the disturbances in a case with a simple model. The second is a Linear State Observer, which is used to estimate a state based on the plant model. Furthermore, in both cases, we have the same proportional-derivative controller after decoupling the dynamics. The main goal of the paper is to examine both controllers for the magnetorheological actuator. Therefore, the designed control systems are verified in a series of experiments.

Keywords: active disturbance rejection control; magnetorheological elastomer membrane; state estimation; smart actuator

Citation: Czopek, P.; Bernat, J. Design and Analysis of the Model Based Control System for an MRE Axisymmetric Actuator. *Electronics* **2023**, *12*, 4386. https://doi.org/10.3390/electronics12214386

Academic Editors: Mahmut Reyhanoglu, Erkan Kayacan and Mohammad Jafari

Received: 3 September 2023
Revised: 12 October 2023
Accepted: 18 October 2023
Published: 24 October 2023

1. Introduction

The magnetorheological elastomers are widely used in control systems and robotics to create advanced actuators and sensors [1,2]. The material is well known in the design process of isolators and vibration absorbers [1]. However, recently, interesting new actuators have also been created with this material. In papers [2,3], applications of haptic devices, valves, or pumps are shown. There are also applications in robotics such as gripper [3,4].

The purpose of this work is to analyze the control system for the MRE axisymmetric actuator. The actuator, which was presented in work [5], is based on a magnetorheological membrane. The membrane properties were recently deeply studied, for instance in the works [2,3]. Compared to the magnetorheological fluid [6], which is in a liquid state, the magnetorheological elastomer is a membrane. Its main features are its softness and responsiveness to a magnetic field. Therefore, it is possible to create a device controlled by a magnetic field. The device presented in work [5] transforms magnetic energy into displacement. It also uses a permanent magnet to increase the range of movement. To improve the performance of the device, designing a control system was required.

The control problem of a nonlinear plant with single input and single output is a typical problem for actuators. One solution is to apply standard algorithms like PID controllers. Another possibility is to use a Linear State Observer like a Luenberger Observer with a feedback controller [7]. Due to the wide range of robustness to unknown dynamics, the Active Disturbance Rejection Control (ADRC) has becomes popular [8–13]. It consists of an extended state observer, which was successfully applied to many problems [14] and feedback controllers. Another well-analyzed solution is to apply a Linear Extended State Observer (LESO) and linear feedback controller with disturbance rejection. The disturbance signal caused by external and internal imperfections is estimated by an extended variable in the

observer and then applied to the controller to decouple disturbances. The ADRC approach has been successfully applied to multiple control problems in recent times. For example, in the work [15], the path-following controller has been designed for underactuated vehicles. The work [16] shows the application of ADRC in a Quadrotor UAV, and works [17,18] describe an electric machine ADRC system control.

In this work, two schemes of the MRE axisymmetric actuator are analyzed. The main objective of the work is to obtain the controllers for the MRE axisymmetric actuator. The controllers are designed based on the output feedback with state estimation. In this work, we use two different approaches. In the first, the reduced model is used to create an ADRC controller based on the LESO. In the second, the full model is applied to create a state feedback controller with a Lueneberger Observer as the Linear State Observer. In both controllers, the compensator is used to decouple dynamics and to apply the PD controller. To show the properties of both controllers, a wide range of experiments are performed with multiple tuning parameters.

2. Model

In the presented work, a control system with MRE axisymmetric actuator is analyzed. The actuator is based on the soft magnetorheological elastomer with an attached permanent magnet as shown in work [5]. The plant is controlled by an electromagnetic field created by an electromagnet with controlled input voltage. The output is the displacement of the membrane center. In work [5], it is shown that the plant model can be described by the Hammerstein model. The linear part of the model can be split into fast and slow dynamics. The model has a third order with a relative degree of 2 and it is described by:

$$\begin{aligned} Y(s) &= G_{fast}(s)G_{slow}(s)V(s) + D(s) \\ v(t) &= f_{nlr}(u(t)) \end{aligned} \tag{1}$$

where $Y(s)$ is the output, $U(s)$ is the input, $G_{fast}(s)$ is the transfer function of the fast dynamics, $G_{slow}(s)$ is the transfer function of the slow dynamics and $f_{nlr}(u)$ describes the input nonlinearity of the system and $D(s)$ describes external disturbances. The transfer function details are as follows:

$$\begin{aligned} G_{slow}(s) &= \frac{s + z_0}{s + s_0} \\ G_{fast}(s) &= \frac{k\left(\alpha^2 + \omega^2\right)}{s^2 + 2\alpha s + \alpha^2 + \omega^2} \end{aligned} \tag{2}$$

In this work, the controllers are designed based on two different models. In the first, the linear model with slow and fast dynamics is taken into account and the non-linearity is replaced by static gain:

$$\begin{aligned} Y(s) &= G_1(s)U(s) + D_1(s) \\ G_1(s) &= k_{nlr}G_{fast}(s)G_{slow}(s) \end{aligned} \tag{3}$$

where k_{nlr} is static gain linearizing $f_{nlr}(u)$. The disturbance term $d_1(t)$ expresses unmodelled dynamics and external disturbances. Now, the model in state space form is given by:

$$\begin{aligned} \dot{x}_1 &= x_2 \\ \dot{x}_2 &= a_{21}x_1 + a_{22}x_2 + a_{23}x_v + b_1u + d_1 \\ \dot{x}_v &= a_{31}x_1 + a_{33}x_v \\ y &= x_1 \end{aligned} \tag{4}$$

where the parameters a_{ij} and b are based on the transfer function $k_{nlr}G_{fast}(s)G_{slow}(s)$. The parameters of model (6) are as follows:

$$\begin{aligned} b_1 &= k_{nlr}k\left(\alpha^2+\omega^2\right) \\ a_{33} &= -z_0 \\ a_{31} &= a_{33} \\ a_{22} &= -a_{33}-s_0-2\alpha \\ a_{21} &= a_{33}a_{22}-2\alpha s_0-\left(\alpha^2+\omega^2\right) \\ a_{23} &= \frac{a_{21}a_{33}-(\alpha^2+\omega^2)s_0}{a_{31}} \end{aligned} \tag{5}$$

The model can be also represented in the matrix form:

$$\begin{aligned} \dot{\mathbf{x}}_S &= \mathbf{A}_S\mathbf{x}_S+\mathbf{B}_S\mathbf{u}+\mathbf{d}_1 \\ y &= \mathbf{C}\mathbf{x}_S \end{aligned} \tag{6}$$

where:

$$\begin{aligned} \mathbf{A}_S &= \begin{bmatrix} 0 & 1 & 0 \\ a_{21} & a_{22} & a_{23} \\ a_{31} & 0 & a_{33} \end{bmatrix} \quad \mathbf{B}_S = \begin{bmatrix} 0 \\ b_1 \\ 0 \end{bmatrix} \\ \mathbf{C} &= \begin{bmatrix} 1 & 0 & 0 \end{bmatrix} \\ \mathbf{d}_1 &= \begin{bmatrix} 0 & d_1 & 0 \end{bmatrix}^T \\ \mathbf{x}_S &= \begin{bmatrix} x_1 & x_2 & x_v \end{bmatrix}^T \end{aligned} \tag{7}$$

In the second model, only the fast dynamics are taken into account, so the model is given by:

$$\begin{aligned} Y(s) &= G_2(s)U(s)+b_eD_2(s) \\ G_2(s) &= k_{nlr}G_{fast}(s) \end{aligned} \tag{8}$$

where d_2 is the disturbance in the reduced model and b_e is a gain of disturbance.

It is worth mentioning that $G_{slow}(s)$ represents slow dynamics; hence, its influence can be effectively estimated by the extended observer. The model $G_2(s)$ is only second order and it can be represented in state space form:

$$\begin{aligned} \dot{x}_1 &= x_2 \\ \dot{x}_2 &= a_1x_1+a_2x_2+b_2u+b_ed_2 \\ y &= x_1 \end{aligned} \tag{9}$$

where the parameters of model (9) are equal to:

$$\begin{aligned} a_1 &= -\alpha^2-\omega^2 \\ a_2 &= -2\alpha \\ b_2 &= k_{nlr}k\left(\alpha^2+\omega^2\right) \end{aligned} \tag{10}$$

In our work, we use the LESO to observe the disturbance d_2, so the extended state is introduced:

$$\begin{aligned} \dot{x}_1 &= x_2 \\ \dot{x}_2 &= a_1x_1+a_2x_2+b_2u+b_ex_e \\ \dot{x}_e &= \dot{d}_2 \\ y &= x_1 \end{aligned} \tag{11}$$

The second model is also represented in the state space form:

$$\begin{aligned} \dot{\mathbf{x}}_E &= \mathbf{A}_E \mathbf{x}_E + \mathbf{B}_E u + \mathbf{d}_2 \\ y &= \mathbf{C}\mathbf{x}_E \end{aligned} \tag{12}$$

where:

$$\begin{aligned} \mathbf{A}_E &= \begin{bmatrix} 0 & 1 & 0 \\ a_1 & a_2 & b_e \\ 0 & 0 & 0 \end{bmatrix} \quad \mathbf{B}_E = \begin{bmatrix} 0 \\ b_2 \\ 0 \end{bmatrix} \\ \mathbf{d}_2 &= \begin{bmatrix} 0 & 0 & \dot{d}_2 \end{bmatrix}^T \\ \mathbf{x}_E &= \begin{bmatrix} x_1 & x_2 & x_e \end{bmatrix}^T \end{aligned} \tag{13}$$

In both models described by (6) and (12), x_1 is the position and also the output is y, x_2 is the velocity and u is the input voltage. The difference is in the number of parameters required to identify and interpret the third state. In model (6), x_v represents the process of membrane relaxation (the change in force due to the relaxation of force in silicone). In model (12), x_e is the extended state estimating the distribution of unmodeled dynamics.

3. Control Algorithm

Two control algorithms will be described in this section. The first algorithm is based on a feedback regulator with a Linear State Observer. The second algorithm is Active Disturbance Rejection Control based on the Linear Extended State Observer. Models from the previous section are applied to construct the control laws. Both algorithms have the same general block diagram structure, which is shown in Figure 1. The main parts of the control system are the plant, the observer and the controller. The plant has a single input u (voltage applied to electromagnet) and single output y (output distance). The reference signal is specified as:

$$x_r = \begin{bmatrix} x_{1r} & x_{2r} \end{bmatrix}^T = \begin{bmatrix} y_r & \dot{y}_r \end{bmatrix}^T. \tag{14}$$

where y_r is the reference signal (output distance) and $\dot{y}_r$ is its derivative. The controller is based on a Proportional Derivative regulator. The main difference between the algorithms is the state observer.

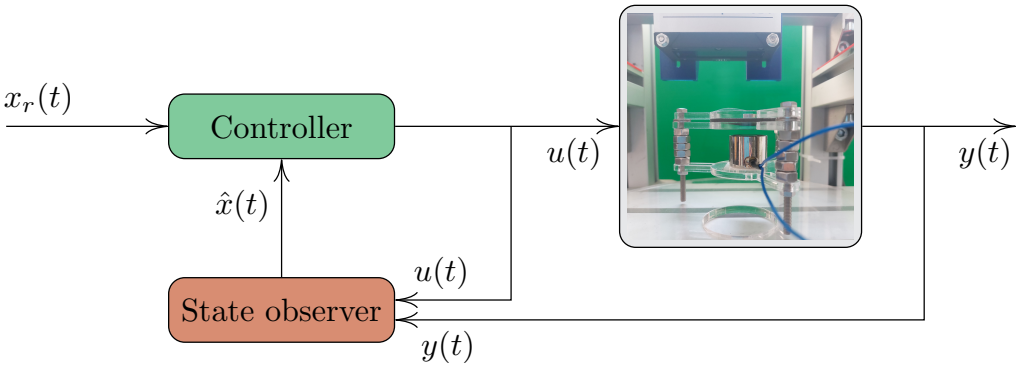

Figure 1. The schema of the control system.

3.1. Linear State Observer

The Linear State Observer is implemented using the model presented in (6). It is based on the Luenberger Observer:

$$\dot{\hat{\mathbf{x}}}_S = \mathbf{A}_S \hat{\mathbf{x}}_S + \mathbf{B}_S u + \mathbf{L}_S(\hat{y} - y) \tag{15}$$

where $\hat{\mathbf{x}}_S$ is estimated state, $\mathbf{L}_S$ is observer gain, $\mathbf{A}_S$ and $\mathbf{B}_S$ are the plant model defined in (6). Luenberger Observer's gains $\mathbf{L}_S$ are calculated to make the matrix eigenvalues $\mathbf{A}_S - \mathbf{L}_S\mathbf{C}$ described by polynomial $(s + \omega_o)^3$. The calculated elements $\mathbf{L}_S$ have the following form:

$$\begin{aligned} l_{s1} &= 3\omega_o + a_{22} + a_{33} \\ l_{s2} &= 3\omega_o^2 + a_{21} - a_{22}a_{33} + a_{22}l_{s1} + a_{31}l_{s1} \\ l_{s3} &= \frac{1}{a_{23}}\left(\omega_o^3 - a_{21}a_{33} + a_{33}l_{s2} - a_{22}a_{33}l_{s1}\right) + a_{31} \end{aligned} \tag{16}$$

where ω_o is the cut-off angular frequency selected by the designer.

We use the estimated state to compensate for disturbance and unknown dynamics for which we define the following control law:

$$u = \frac{1}{b_1}(u^* - a_{21}x_1 - a_{22}\hat{x}_2 - a_{23}\hat{x}_v) \tag{17}$$

where u is the control signal applied to the plant and u^* is the PD controller signal.

3.2. Linear Extended State Observer

In the second control algorithm, we used the Linear Extended-State Observer (LESO) to estimate plant state with extended state represent disturbance. The LESO can be written as:

$$\dot{\hat{\mathbf{x}}}_E = \mathbf{A}_E\hat{\mathbf{x}}_E + \mathbf{B}_E u + \mathbf{L}_E(\hat{y} - y) \tag{18}$$

We use the Linear Extended State Observer, for which we define the gain $L_E = \begin{bmatrix} l_{e1} & l_{e2} & l_{e3} \end{bmatrix}^T$ and the elements of the vector as:

$$\begin{aligned} l_{e1} &= 3\omega_o + a_2 \\ l_{e2} &= 3\omega_o^2 + l_{e1}a_2 + a_1 \\ l_{e3} &= \frac{\omega_o^3}{b_2} \end{aligned} \tag{19}$$

where ω_o is the cut-off angular frequency range. To eliminate disturbance and known dynamics, the control law can be written as:

$$u = \frac{u^* - b_e\hat{x}_e - a_1x_1 - a_2\hat{x}_2}{b_2} \tag{20}$$

3.3. PD Controller

In this part, we show how the PD controller is applied to the MRE Axisymmetric actuator. We consider the plant with an applied compensator based on the estimated state with LSO or LESO. Using (17) or (20) we can simplify the dynamics of the object as seen by the controller to:

$$\begin{aligned} \dot{x}_1 &= x_2 \\ \dot{x}_2 &= u^* \end{aligned} \tag{21}$$

The selected controller is a proportional derivative with a feed-forward loop regulator (PD+FF) described by:

$$u^* = k_p(x_1 - x_{1r}) + k_d(\hat{x}_2 - x_{2r}) - \ddot{y}_r \tag{22}$$

where x_r is the reference signal, k_p and k_d are controller gains which are chosen to have poles located as $\omega_c\left(\frac{\sqrt{2}}{2} \pm j\frac{\sqrt{2}}{2}\right)$; hence,

$$\begin{aligned} k_p &= -\omega_c^2 \\ k_d &= -\sqrt{2}\omega_c. \end{aligned} \tag{23}$$

The cut-off angular frequency ω_c is provided by the designer. The signal u^* is given in the compensation loop to calculate the u signal. The states x_1 and x_2 have the same interpretation, so the controller is the same for both control algorithms.

3.4. Stability Analysis

The next step is stability analysis which is performed based on the models and control laws defined before. The Nyquist stability criterion for an open-loop system is applied to calculate whether the system is stable or not. Therefore, it is required to calculate the open-loop system transfer function defined as:

$$G_{open}(s) = G_{ctr}(s)G_{plant}(s) \tag{24}$$

where $G_{open}(s)$ is the open-loop transfer function, $G_{ctr}(s)$ is the controller open-loop transfer function and $G_{plant}(s)$ is the plant transfer function. In our work, we have two cases. In both cases, the plant is defined as (3), whereas the transfer function of controller $G_{ctr}(s)$ can be calculated from the state space representation of (15), (17) and (22). In the case of LSO and PD controller, the state space can be specified as:

$$\begin{aligned} \dot{\hat{\mathbf{x}}}_S &= (\mathbf{A}_S - \mathbf{L}_S\mathbf{C} + \mathbf{B}_S\mathbf{K}_\mathbf{S}^\mathbf{e})\hat{\mathbf{x}}_S - (\mathbf{L}_S + \mathbf{B}_S\mathbf{K}_\mathbf{S}^\mathbf{o})y_o \\ u &= \mathbf{K}_\mathbf{S}^\mathbf{e}\hat{x}_S - \mathbf{K}_\mathbf{S}^\mathbf{o}y_o \end{aligned} \tag{25}$$

where y_o is the open-loop input for the controller (in closed loop equal to $y_o = -y$) and u is the output of the controller. The gains $\mathbf{K}_\mathbf{S}^\mathbf{e}$ and $\mathbf{K}_\mathbf{S}^\mathbf{o}$ are calculated from (17) and (22):

$$\mathbf{K}_\mathbf{S}^\mathbf{e} = \begin{bmatrix} 0 & \frac{k_d - a_{22}}{b_1} & -\frac{a_{23}}{b_1} \end{bmatrix} \quad \mathbf{K}_\mathbf{S}^\mathbf{o} = \begin{bmatrix} \frac{k_p - a_{21}}{b_1} \end{bmatrix} \tag{26}$$

Similarly, the LESO with PD controller based on (18), (20) and (22) is as follows:

$$\begin{aligned} \dot{\hat{\mathbf{x}}}_E &= (\mathbf{A}_E - \mathbf{L}_E\mathbf{C} + \mathbf{B}_E\mathbf{K}_\mathbf{E}^\mathbf{e})\hat{\mathbf{x}}_E - (\mathbf{L}_E + \mathbf{B}_E\mathbf{K}_\mathbf{E}^\mathbf{o})y_o \\ u &= \mathbf{K}_\mathbf{E}^\mathbf{e}\hat{x}_E - \mathbf{K}_\mathbf{E}^\mathbf{o}y_o \end{aligned} \tag{27}$$

where gains

$$\mathbf{K}_\mathbf{E}^\mathbf{e} = \begin{bmatrix} 0 & \frac{k_d - a_2}{b_2} & -\frac{b_e}{b_2} \end{bmatrix} \quad \mathbf{K}_\mathbf{E}^\mathbf{o} = \begin{bmatrix} \frac{k_p - a_1}{b_2} \end{bmatrix} \tag{28}$$

The form represented in (25) and (27) allows us to simply calculate the transfer function with the help of numerical packages. In the simulation section, the Nyquist plots of both controllers will be shown.

4. Experiments

This section describes the experimental verification of the designed controllers. The quality of controllers was examined on the MRE Axisymmetric actuator described in work [5]. In this section, the hardware description, stability analysis and experimental tests will be shown.

The hardware used to perform experiments was equipped with the controller unit, power driver and feedback sensor. Control algorithms were implemented on the Nucleo STM32 microcontroller. We also used an H-bridge as an extended device to energize the electromagnet coil. The coil generated an electromagnetic field that moved the membrane. The power supply was the pulse wave modulation signal (PWM) with an amplitude of −12

to 12 V. Above the membrane is the laser sensor (Micro-Epsilon ILD1900-25), for which we built an electrical system to supply and convert laser output to the microcontroller input.

Now, the model parameters and stability analysis will be described. The actuator parameters are based on the previous works and are specified in Table 1. It is visible that the system has a single stable zero, a slow real pole and a fast complex pole.

Table 1. Plant model parameters from work [5].

Name	Parameter	Value	Unit
nonlinear gain	k_{nlr}	-0.08241	$\mathrm{mm\,V^{-1}}$
linear gain	k	0.77	1
zero	z_0	0.18	1/s
pole	s_0	0.14	1/s
decay rate	α	32.91	1/s
angular frequency	ω	218.98	$\mathrm{rads^{-1}}$

The stability is analyzed by the Nyquist criterion based on the open-loop transfer function (24). The results of the Nyquist stability criterion are shown in Figure 2. The open-loop systems are stable, and as visible in Figure 2, both systems are stable and have similar Nyquist plots. The figure shows also the stability under a small time delay ($\tau_d = 2\,\mathrm{ms}$). It is clear that time delay has a great influence on systems with higher ω_c. Additionally, the stability margins are calculated for the presented system and shown in Table 2.

Table 2. Stability margins for the controllers with LSO and LESO observers.

Observer	$\omega_c(\mathrm{rads^{-1}})$	Delay	Gain Margin	Phase Margin
LSO	100	0 ms	1.78	56.11
LSO	100	2 ms	1.76	53.03
LSO	200	0 ms	7.41	78.30
LSO	200	2 ms	2.11	44.61
LESO	100	0 ms	1.78	55.71
LESO	100	2 ms	1.76	52.62
LESO	200	0 ms	7.40	78.25
LESO	200	2 ms	2.10	44.56

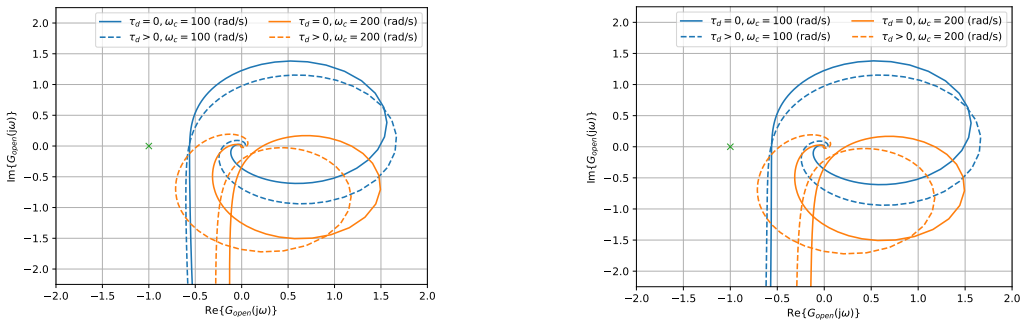

(**a**) (**b**)

Figure 2. The Nyquist plot with stability criterion. (**a**) PD Controller with Linear State Observer. (**b**) PD Controller with Linear Extended State Observer.

To verify the controller, experiments showing its tracking possibilities were conducted. The series of cut-off frequencies were tested to show the influence on different observer and control gains:

- $\omega_o = \{275, 350, 425, 500, 575\}\ \mathrm{rads^{-1}}$
- $\omega_c = \{100, 200\}\ \mathrm{rads^{-1}}$

We test control algorithms for the sinusoidal reference signal described by:

$$y_r(t) = A_r \sin(2\pi f_r t) \tag{29}$$

where $A_r = 0.3$ mm is amplitude, f_r is frequency equal 5 Hz. The single test lasts 15 s and the probe time is set at $T_p = 1$ ms. The example results of experiments are presented in Figures 3 and 4, where are illustrated: reference signal y_r, measure position y and estimated position $\hat{y}$. On the graph waveforms, we can see a noise impact in y and $\hat{y}$ signals, and we can also see that the estimated position is very close to the measured position. For the sets $\omega_c = 100$ rads^{-1} and $\omega_o = 500$ rads^{-1}, the control quality is acceptable, but there is a slight delay between y_r and y. Changing ω_c to 200 rads^{-1} reduced the signal delay but increased the noise.

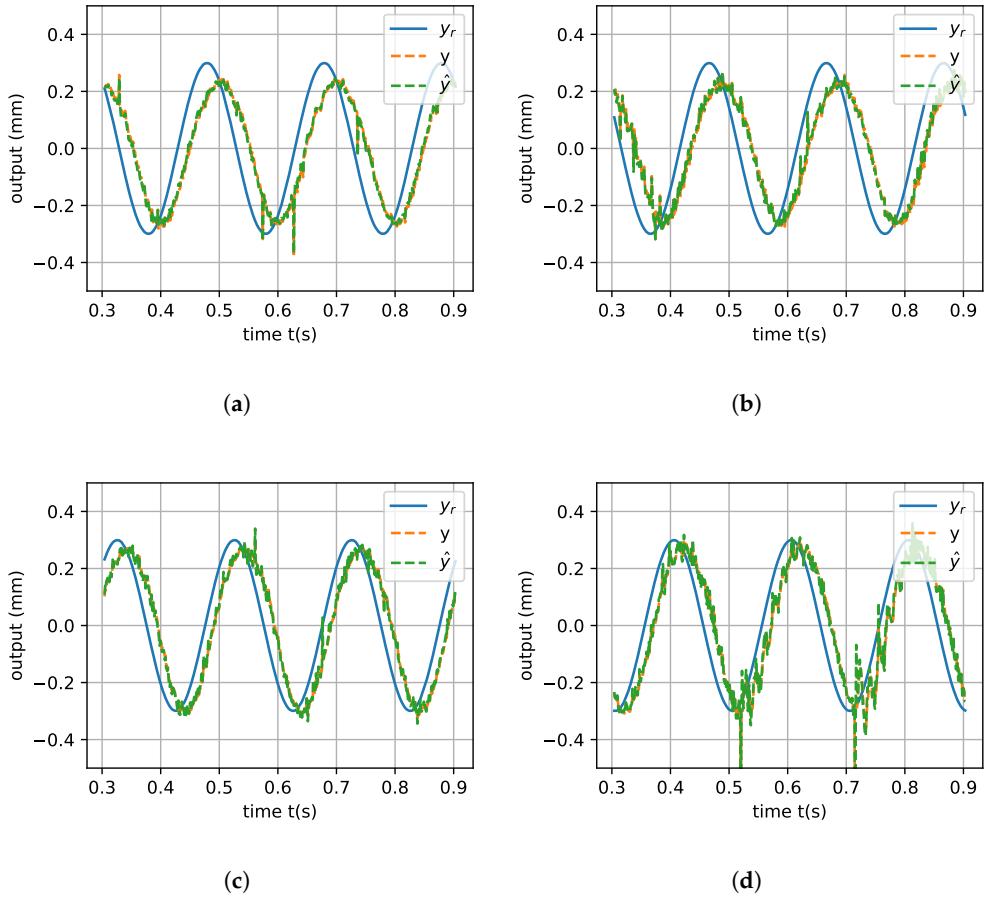

Figure 3. The membrane position in time for $A_r = 0.3$ mm, $f_r = 5$ Hz, $\omega_c = 100$ rads^{-1} and different ω_o. On the left side is the control algorithm with the Linear State Observer (LSO) (**a**,**c**), whereas on the right side is the control algorithm with the Linear Extended State Observer (LESO) (**b**,**d**). (**a**) $\omega_o = 350$ rads^{-1}. (**b**) $\omega_o = 350$ rads^{-1}. (**c**) $\omega_o = 500$ rads^{-1}. (**d**) $\omega_o = 500$ rads^{-1}.

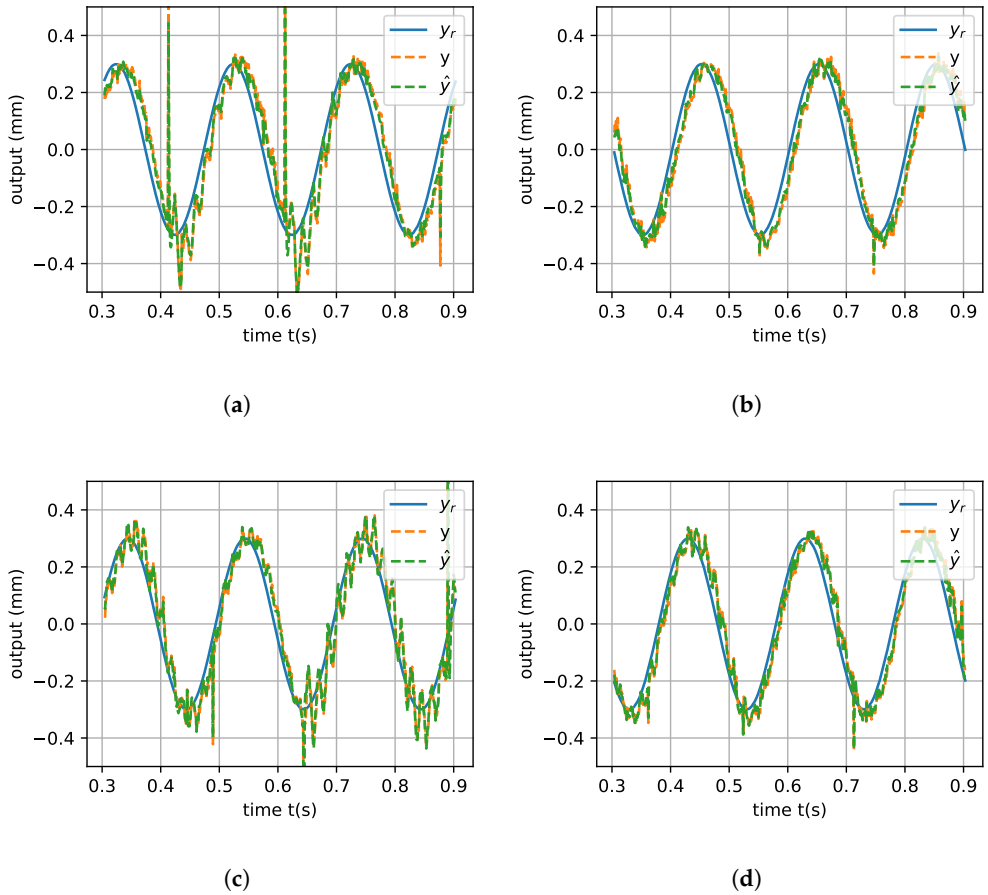

Figure 4. The membrane position in time for $A_r = 0.3$ mm, $f_r = 5$ Hz, $\omega_c = 200$ rads^{-1} and different ω_o. On the left side is the control algorithm with the Linear State Observer (**a**,**c**), whereas on the right side is the control algorithm with the Linear Extended State Observer (**b**,**d**). (**a**) $\omega_o = 275$ rads^{-1}. (**b**) $\omega_o = 275$ rads^{-1}. (**c**) $\omega_o = 350$ rads^{-1}. (**d**) $\omega_o = 350$ rads^{-1}.

5. Discussion

The results obtained in the experiments are analyzed and discussed with auxiliary tools to obtain more insight into the results. Firstly, control algorithms were also analyzed using the Integral Square Error described:

$$J_{ISE} = \int_0^T [y(\tau) - y_r(\tau)]^2 d\tau \tag{30}$$

where T is the final time of the experiment. Values of J_{ISE} for different control algorithms and different parameter values are presented in Figure 5. In this figure, we present data from two experimental trials. Analyzing results from the first trial and the second trial, it can be seen that the values of J_{ISE} are similar, respectively, and speak to the experiments that are repetitive. The optimal results for the LESO algorithm and the LSO algorithm are for parameters $\omega_c = 100$ rads^{-1} and $\omega_o = 575$ rads^{-1}. For these parameter values, the system control achieves a high accuracy control. For these parameter values, where the system was unstable, J_{ISE} reach high values. These parameters are $\omega_c = 200$ rads^{-1} and $\omega_o = \{425, 500, 575\}$ rads^{-1}.

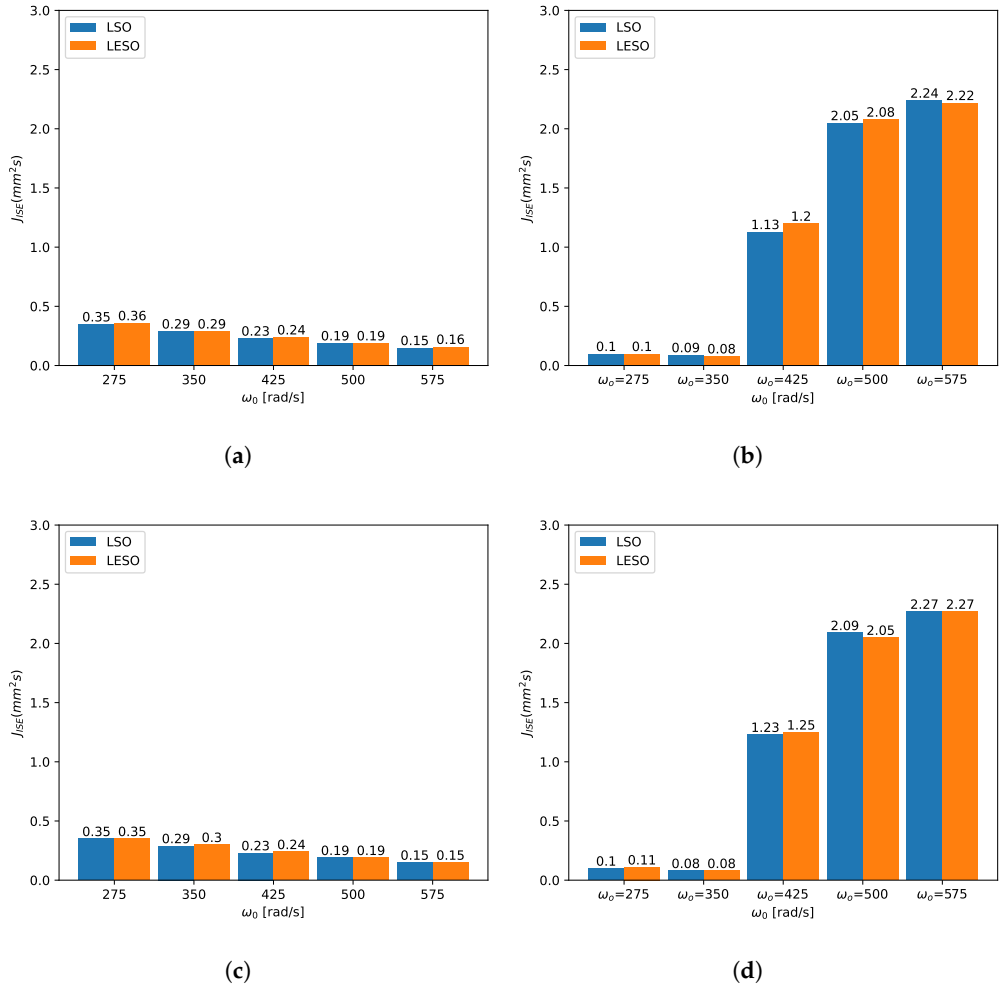

Figure 5. The values of J_{ISE} for two trial. The (**a**,**b**) are for the first trial and (**c**,**d**) are for the second trial. (**a**) $\omega_c = 100$ rads^{-1}. (**b**) $\omega_c = 200$ rads^{-1}. (**c**) $\omega_c = 100$ rads^{-1}. (**d**) $\omega_c = 200$ rads^{-1}.

Secondly, the steady state response of the actuator was analyzed in the frequency domain. The power of reference signal, output and noise are calculated as:

$$\begin{aligned} P_{reference} &= A^2_{reference}(f_r) \\ P_{output} &= A^2_{output}(f_r) \\ P_{noise} &= \sum_{f \neq f_r} A^2_{output}(f) \end{aligned} \tag{31}$$

where $P_{reference}$ is the power of reference signal, P_{output} is the power of output signal without noise, P_{noise} is the power of noise of output signal. $A_{reference}$ and A_{output} are amplitude coefficients for a spectrum of frequencies calculated by discrete FFT transformation in the steady state with a window equal to ten periods of reference signal ($T_{window} = \frac{10}{f_r}$). In Figure 6, the power of signals is analyzed for varying cut-off frequencies. It is visible that for low controller cut-off angular frequency, the noise is kept low and the quality of control depends on observer cut-off angular frequency. In the case of high controller cut-off angular frequency, the noise is dominating.

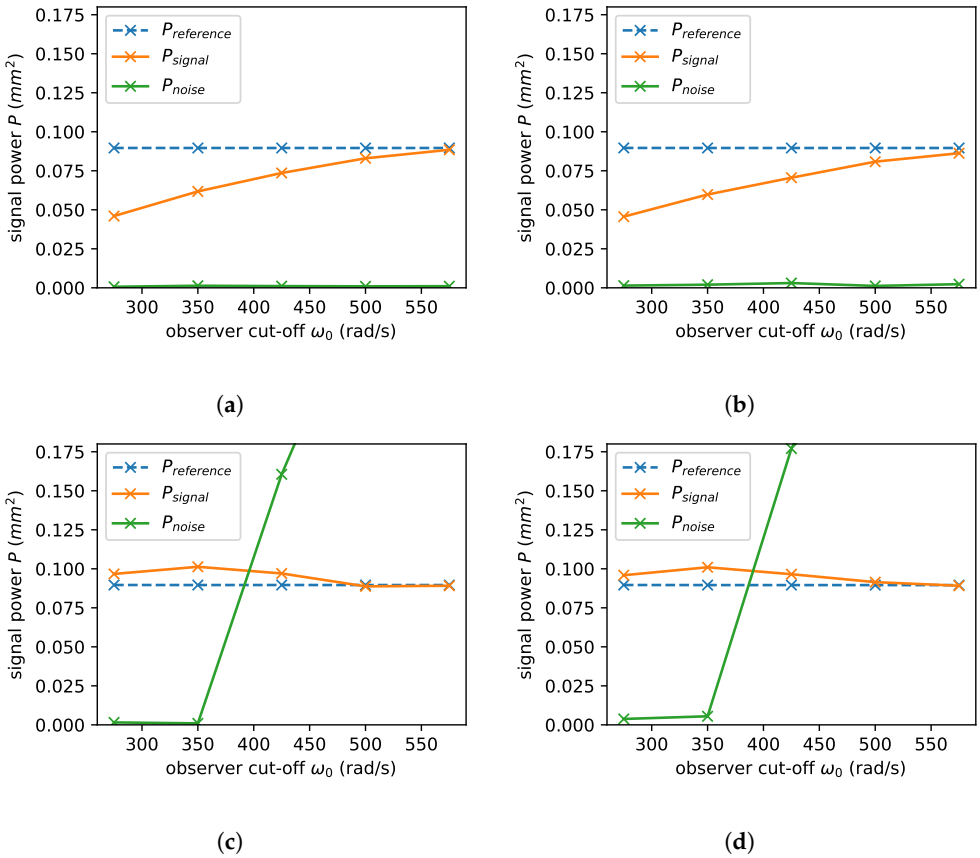

Figure 6. The power of output signal, noise signal and the reference signal for various ω_o for the controller with different state estimation algorithms. Controller with Linear State Observer (**a**,**c**), Controller with Linear Extended State Observer (**b**,**d**). (**a**) w_c =100 rad s^{-1}, with LSO. (**b**) w_c =100 rad s^{-1}, with LESO. (**c**) w_c =200 rad s^{-1}, with LSO. (**d**) w_c =200 rad s^{-1}, with LESO.

6. Conclusions

In summary, we analyzed the two types of controllers working in the closed-loop system to control the MRE axisymmetric membrane with a permanent magnet. The first was implemented based on a Linear State Observer with a Luenberger Observer and using information about slow and fast plant dynamics. The second was implemented as ADRC with a Linear Extended State Observer using a reduced model with knowledge about only fast dynamics. Then, we tested these algorithms in experiments for many variants of parameter values. Both algorithms have similar control quality. FFT analysis has shown that noise has had a crucial impact on control performance. Further, the performance indexes depend strictly on observer and controller cut-off frequencies. In future works, magnetorheological elastomers with the designed controller can be used to construct intelligent actuators, for example, pumps with a variable capacity of chambers.

Author Contributions: Conceptualization, P.C. and J.B.; software, P.C.; investigation, P.C. and J.B.; formal analysis, P.C. and J.B.; visualization, P.C.; writing—original draft preparation, P.C. and J.B.; writing—review and editing, P.C. and J.B.; supervision, J.B. All authors have read and agreed to the published version of the manuscript.

Funding: This research was funded by the Ministry of Education and Science, grant number 0211/SBAD/0123.

Data Availability Statement: Data sharing not applicable.

Conflicts of Interest: The authors declare no conflict of interest.

References

1. Li, Y.; Li, J.; Li, W.; Du, H. A state-of-the-art review on magnetorheological elastomer devices. *Smart Mater. Struct.* **2014**, *23*, 123001. [CrossRef]
2. Böse, H.; Gerlach, T.; Ehrlich, J. Magnetorheological elastomers—An underestimated class of soft actuator materials. *J. Intell. Mater. Syst. Struct.* **2021**, *32*, 1550–1564. [CrossRef]
3. Bernat, J.; Gajewski, P.; Kołota, J.; Marcinkowska, A. Silicone-Based Membranes as Potential Materials for Dielectric Electroactive Polymer Actuators. *Energies* **2022**, *15*, 6324. [CrossRef]
4. Guan, R.; Zheng, H.; Liu, Q.; Ou, K.; Li, D.-s.; Fan, J.; Fu, Q.; Sun, Y. DIW 3D printing of hybrid magnetorheological materials for application in soft robotic grippers. *Compos. Sci. Technol.* **2022**, *223*, 109409. [CrossRef]
5. Bernat, J.; Superczynska, P.; Gajewski, P.; Marcinkowska, A. Magnetorheological Axisymmetric Actuator with Permanent Magnet. *arXiv* **2022**, arXiv:2210.15968. https://doi.org/10.48550/ARXIV.2210.15968.
6. Ashour, O.; Rogers, C.A.; Kordonsky, W. Magnetorheological Fluids: Materials, Characterization, and Devices. *J. Intell. Mater. Syst. Struct.* **1996**, *7*, 123–130. [CrossRef]
7. Hendricks, E.; Jannerup, O.; Sørensen, P. *Linear Systems Control: Deterministic and Stochastic Methods*; Springer: Berlin/Heidelberg, Germany, 2008.
8. Huang, Y.; Xue, W. Active disturbance rejection control: Methodology and theoretical analysis. *ISA Trans.* **2014**, *53*, 963–976. [CrossRef] [PubMed]
9. Yoo, D.; Yau, S.T.; Gao, Z. Optimal fast tracking observer bandwidth of the linear extended state observer. *Int. J. Control* **2007**, *80*, 102–111. [CrossRef]
10. Han, J. From PID to active disturbance rejection control. *IEEE Trans. Ind. Electron.* **2009**, *56*, 900–906. [CrossRef]
11. Herbst, G. A Simulative Study on Active Disturbance Rejection Control (ADRC) as a Control Tool for Practitioners. *Electronics* **2013**, *2*, 246–279. [CrossRef]
12. Pazderski, D.; Patelski, R.; Krysiak, B.; Kozłowski, K. Analysis of an Impact of Inertia Parameter in Active Disturbance Rejection Control Structures. *Electronics* **2020**, *9*, 1801. [CrossRef]
13. Patelski, R.; Pazderski, D. Improving the Active Disturbance Rejection Controller Tracking Quality by the Input-Gain Underestimation for a Second-Order Plant. *Electronics* **2021**, *10*, 907. [CrossRef]
14. Haroon, S.I.A.; Qian, J.; Zeng, Y.; Zou, Y.; Tian, D. Extended State Observer Based-Backstepping Control for Virtual Synchronous Generator. *Electronics* **2022**, *11*, 2988. [CrossRef]
15. Łakomy, K.; Michałek, M.M. Robust output-feedback VFO-ADR control of underactuated spatial vehicles in the task of following non-parametrized paths. *Eur. J. Control* **2021**, *58*, 258–277. [CrossRef]
16. Cheng, Y.; Dai, L.; Li, A.; Yuan, Y.; Chen, Z. Active Disturbance Rejection Generalized Predictive Control of a Quadrotor UAV via Quantitative Feedback Theory. *IEEE Access* **2022**, *10*, 37912–37923. [CrossRef]
17. Zhang, C.; Zhang, C.; Li, L.; Liu, H. An Enhanced Nonlinear ADRC Speed Control Method for Electric Propulsion System: Modeling, Analysis, and Validation. *IEEE Trans. Power Electron.* **2023**, *38*, 4520–4528. [CrossRef]
18. Shi, S.; Guo, L.; Chang, Z.; Zhao, C.; Chen, P. Current Controller Based on Active Disturbance Rejection Control With Parameter Identification for PMSM Servo Systems. *IEEE Access* **2023**, *11*, 46882–46891. [CrossRef]